Chemical Geology 345 (2013) 113–118

Contents lists available at SciVerse ScienceDirect

Chemical Geology

journal homepage: www.elsevier.com/locate/chemgeo

Thermal effects of scanning electron microscopy on He diffusion in apatite: Implications for (U–Th)/He dating

Jingnan Shan [a,b], Kyoungwon Min [b,*], Abdelkader Nouiri [c]

[a] Institute of Geology and Geophysics, Chinese Academy of Sciences, Beijing, 100029, China
[b] Department of Geological Sciences, University of Florida, Gainesville, FL 32611, USA
[c] Material Sciences Department, University Oum EI-Bouaghi, Oum EL-Bouaghi, 04000, Algeria

ARTICLE INFO

Article history:
Received 3 August 2012
Received in revised form 1 March 2013
Accepted 7 March 2013
Available online 15 March 2013

Editor: K. Mezger

Keywords:
Scanning electron microscope (SEM)
(U–Th)/He dating
Durango apatite
Temperature rise
He diffusion

ABSTRACT

In order to investigate potential diffusive loss of He from apatites during SEM analysis, we performed (1) single-grain (U–Th)/He dating for 47 Durango apatite fragments (from <90 μm to 150–250 μm) which were previously examined using SEM under different analytical conditions, and (2) electron–matter interaction simulation combined with diffusion modeling. The determined (U–Th)/He ages are internally consistent within their errors, and indistinguishable from the reported $^{40}Ar/^{39}Ar$ ages of 31.44 ± 0.18 (2σ) Ma and the apatite (U–Th)/He ages of 31.02 ± 1.01 Ma (Standard Deviation; McDowell et al., 2005). The results from the electron–matter interaction simulation suggest that "temperature rise" (ΔT = temperature increase during electron bombardment) peaks within a very thin layer at the outermost of the hypothetical apatite grain, and falls below ~50 K within a depth of 0.3 μm from the surface. Based on the simulated ΔT profile combined with available He diffusion parameters, the fractional loss of He (f_{He}) was calculated for different apatite grain dimensions. The numerical simulation supports that the He loss from apatite grains of typical physical dimensions is negligible (<1%) under regular SEM operating conditions. The direct measurements of (U–Th)/He ages for SEM-treated apatites, as well as diffusion simulation using the electron–matter interaction model, indicate that SEM spot analysis or extensive chemical mapping prior to apatite (U–Th)/He dating does not cause any meaningful diffusive He loss for most of the apatite samples.

1. Introduction

A scanning electron microscope (SEM) provides one of the most popular analytical methods for describing surface morphologies and chemical compositions for a wide range of solid materials. Because the modern SEM is capable of producing high resolution imaging even for uncoated samples, it is commonly used for characterizing samples prior to more advanced analytical procedures which, in many cases, are subject to invasive and destructive analyses that cause significant modifications of the samples' original features. In many fields of Earth and Planetary Sciences, it has become a routine procedure to examine natural samples using SEM, along with such various applications as identifying minerals with a spot analysis or obtaining detailed chemical maps using EDS (energy dispersive spectroscopy); examining grain surface topography or intragrain fracture patterns using SE (secondary electron) mode; and characterizing chemical zoning using BSE (back-scattered electron) or CL (cathodoluminescent) mode. For a range of *in-situ* analytical procedures (e.g., SHRIMP, LA-ICP-MS, laserprobe $^{40}Ar/^{39}Ar$ and (U–Th)/He), it is critical to avoid any inclusions and to find optimal locations in the samples, and SEM provides the most efficient way to achieve these purposes. Furthermore, for such precious samples as meteorites, it is important to thoroughly describe the samples before major analytical procedures (Min et al., 2004; Hudgins et al., 2008).

The fundamental assumption for many of these applications is that SEM analysis produces minimal, if any, modifications to the original nature of the samples, therefore those same samples can be used in further investigations. Although this assumption could well be tenable for the majority of cases, some applications may require more thorough testing of this assumption, particularly when the results can be easily biased by a mild thermal disturbance during SEM analysis. For example, argon diffusion in specific phases, such as K-feldspar and glass, is sensitive to temperatures induced by routine SEM analysis, possibly yielding biased $^{40}Ar/^{39}Ar$ ages (Flude et al., 2010). A similar concern has been raised regarding (U-Th)/He thermochronometry on apatite, in which He diffusion is known to be even more sensitive to temperatures than Ar diffusion in K-feldspar (Zeitler et al., 1987).

During SEM analysis, interactions between the incident electrons from the source and atomic elections within the sample cause a temperature increase (ΔT) by transforming a certain amount of kinetic energy into heat in the sample (Talmon and Thomas, 1977, 1978). Numerical simulations for this process were provided (Mirkarimi et al., 2002; Randolph et al., 2005; Nouiri et al., 2006), and we employed

* Corresponding author. Tel.: +1 352 392 2231; fax: +1 352 392 9294.
E-mail address: kmin@ufl.edu (K. Min).

0009-2541/$ – see front matter © 2013 Elsevier B.V. All rights reserved.
http://dx.doi.org/10.1016/j.chemgeo.2013.03.001

this approach to estimate ΔT in terrestrial apatites during SEM analysis. In this contribution, we aim to evaluate such effects through two independent approaches: (1) determining (U–Th)/He ages of Durango apatite grains that have previously undergone examination under different SEM analytical conditions, and (2) estimating electron-beam induced ΔT by simulating the random walk behavior of electrons in apatite, followed by diffusion modelling. Although the main focus of this study is He diffusion in apatite, a similar approach can be easily extended to other systems.

2. Methods

2.1. (U–Th)/He dating

In order to investigate the potential causal effect of SEM analysis on He diffusion in apatite, we examined multiple fragments of Durango apatite using SEM under different analytical conditions, then determined their single-grain (U–Th)/He ages. The Durango apatite is one of the most widely used standards in the (U-Th)/He community, and its precise (U–Th)/He ages (McDowell et al., 2005), He diffusion properties (Wolf et al., 1996, 1997; Farley, 2000; Shuster et al., 2003), and intragrain U-Th distributions (Boyce and Hodges, 2005) have been investigated in detail.

The first set of samples (batch 1) was examined for any evidence of disturbed (U-Th)/He ages from three size fractions of Durango apatite (<90 μm, 90–150 μm and 150–250 μm), which were mounted on two different materials (copper and regular adhesive tapes), and analyzed for two SEM analytical durations (6.4 and 25.6 minutes). For this test, a large Durango apatite crystal was carefully crushed into fragments, which were sieved and divided into three size groups: <90 μm, 90–150 μm and 150–250 μm. Most apatite fragments were angular shards, thus the fragments in the same size groups had a range of morphologies, with some of their linear dimensions exceeding the specified size limits. To avoid this size effect, we tried to select grains with similar physical dimensions in the same size fractions. A total of 23 fragments were examined under a stereomicroscope and divided into four subgroups (named as Subgroups 1–4), each of which was composed of 5–7 grains of different size fractions. The fragments were mounted on copper tape (Subgroups 1 and 3) or on regular adhesive tape (Subgroups 2 and 4) to investigate any differences between the two common mounting materials. The samples were analyzed using the Zeiss EVO-MA10 variable pressure SEM at the University of Florida. Individual grain fragments were examined with a secondary electron (SE) mode to observe basic surface features, then chemically mapped with Energy Dispersive Spectroscopy (EDS) under constant operating conditions (Table 1). To examine any effects from scanning durations, sample fragments in Subgroups 1 and 2 were exposed to the electron beam for 6.4 min, whereas those in Subgroups 3 and 4 for 25.6 min.

As discussed in the following sections, there are essentially no differences in (U-Th)/He ages for the four subgroups comprising batch 1, suggesting that diffusive He loss at the given SEM analytical conditions is negligible. To further investigate potential He diffusion for a wider range of SEM analytical conditions, we prepared another set of Durango apatite fragments (batch 2). Twenty-four Durango apatite fragments of uniform-size (150–250 μm) were selected, divided into four subgroups (identified as Subgroups 5–8), then mounted on a regular adhesive tape for SEM analysis. The fragments were bombarded by the electron-beam with varying probe currents (250–1000 pA) and scanning durations (25.6–120 min) at a constant accelerating energy (EHT target voltage: 16.5 kV), as summarized in Table 1. Individual grains in the same subgroup were analyzed under the same SEM conditions. All of the (U–Th)/He age determinations were performed at the University of Florida (see Appendix for detailed analytical procedures). The ages are reported with 2σ errors, unless otherwise specified.

Table 1
SEM analytical conditions used in this study.

SEM parameter	Batch 1 Subgroups				Batch 2 Subgroups			
	1	2	3	4	5	6	7	8
Probe current [pA]	1000	1000	1000	1000	250	500	750	1000
Scanning duration [min]	6.4	6.4	25.6	25.6	25.6	25.6	60	120
Chamber pressure [Pa]	40	40	40	40	60	60	60	60

Following parameters are set to be constant: Filament I target = 2.66 Amp; Accelerating voltage = 16.5 kV.

2.2. Electron–matter interaction simulation

The electron–matter interaction during SEM analysis may result in a range of effects on incident electrons, which can be divided into two primary types of electron scattering: elastic and inelastic (Egerton et al., 2004). Among these, only the inelastic scattering (i.e. excitation of lattice oscillations) is expected to generate phonons leading to substantial heating in the sample. The resulting ΔT in samples can be estimated based on the hybrid simulation method (Nouiri et al., 2006), which primarily relies on statistics of phonons produced during the random walk process of the incident electrons within the sample.

Generally, the simulation was performed with the following steps: (1) defining numerous random pathways of the incident electrons in the sample over the entire period, from "in" until "out"; (2) dividing the sample into several zones; (3) estimating the number of phonons generated within each zone based on the conditions of the incident electron beam (e.g., accelerating voltage, primary current and scanning time); (4) converting the phonon increment into ΔT in each zone based on thermodynamic laws; and (5) estimating conductive heat loss effects to correct the estimated ΔT. Although our simulation is based on an assumption that an apatite unit cell behaves as a smallest scattering body, further scattering simulation down to an atomic scale is expected to yield almost identical results. More detailed calculation procedures and explanations are available in Nouiri et al. (2006).

3. Results and discussion

3.1. (U–Th)/He dating

From the first batch (Subgroups 1–4), we obtained 23 (U-Th)/He ages ranging from 30.0 ± 1.8 Ma to 33.4 ± 2.2 Ma (Fig. 1 and Table 2). The weighted means for the four subgroups are: 30.9 ± 0.9 Ma (Subgroup 1, n = 5); 31.3 ± 0.8 Ma (Subgroup 2, n = 6); 30.9 ± 0.9 Ma (Subgroup 3, n = 5); and 30.7 ± 0.9 Ma (Subgroup 4, n = 7). These results are indistinguishable within their uncertainties, suggesting that the mounting materials (copper and regular adhesive tapes) and sample dimensions (<90 μm, 90–150 μm and 150–250 μm) did not cause any detectable differences in the resulting (U–Th)/He ages. Furthermore, these ages are in good agreement with the reference ages of the Durango samples: sanidine-anorthoclase $^{40}Ar/^{39}Ar$ age of 31.44 ± 0.18 (2σ) Ma (McDowell et al., 2005); apatite (U–Th)/He ages of 31.02 ± 1.01 Ma (Standard Deviation; n = 24; McDowell et al., 2005), 32.1 ± 1.1 Ma (S.D.; n = 156; Min et al., 2006) and 30.0 ± 0.9 Ma (S.D.; n = 17; Spiegel et al., 2009); and apatite Pb/Pb LA-ICP-MS age of 30.6 ± 2.3 Ma (2σ) (Chew et al., 2011).

The second batch of samples (Subgroups 5–8), which experienced more diverse SEM analytical conditions (Table 1), yield 24 reliable (U–Th)/He ages (Table 3). Their apatite (U–Th)/He ages range from 28.7 ± 1.0 Ma to 33.1 ± 1.6 Ma, with weighted means of 31.2 ± 0.9 Ma (Subgroup 5, n = 8); 30.2 ± 0.9 Ma (Subgroup 6, n = 6); 30.8 ± 1.0 Ma (Subgroup 7, n = 5); and 30.5 ± 1.1 Ma (Subgroup 8,

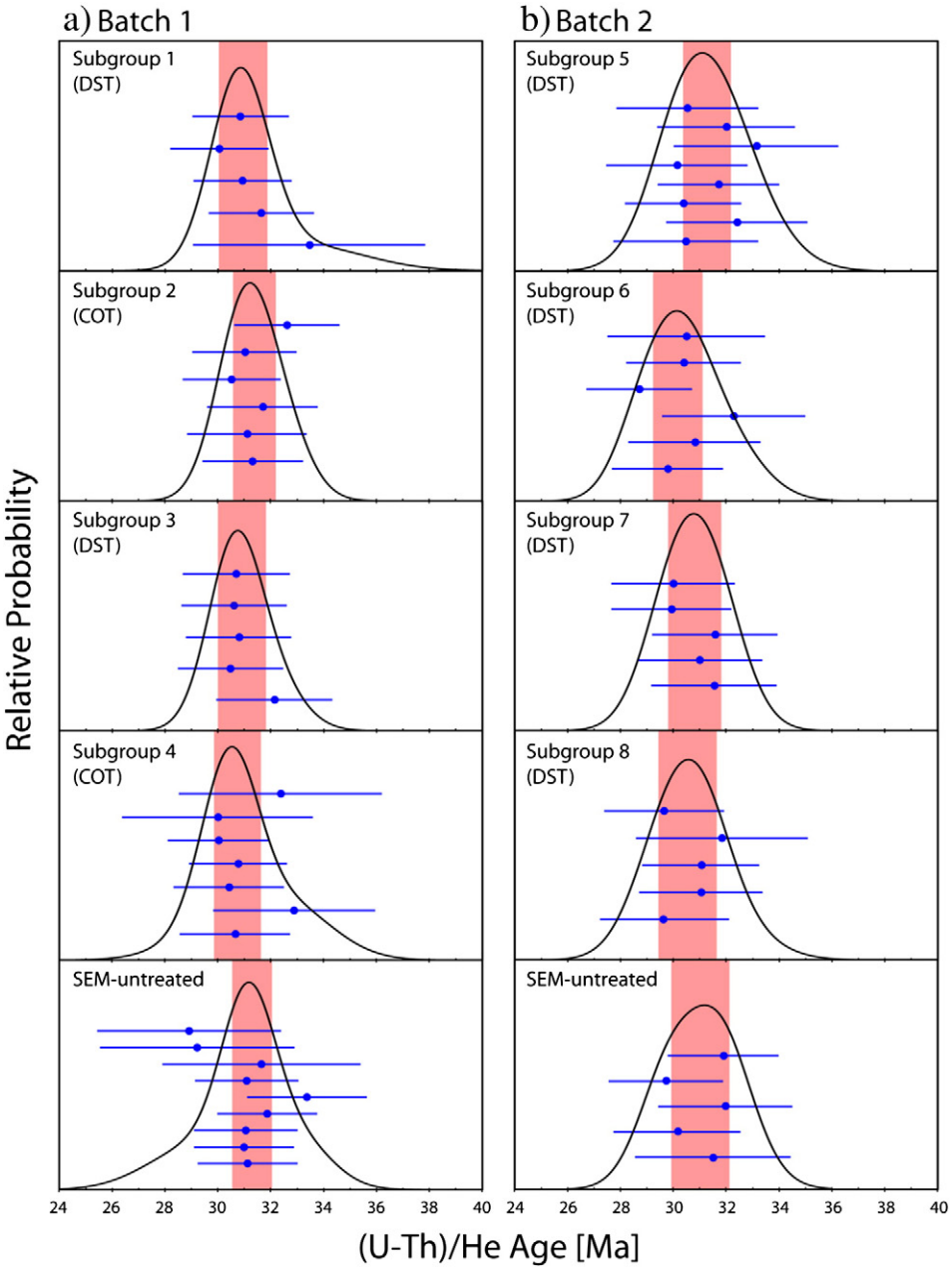

Fig. 1. Probability density plots for single-grain (U–Th)/He ages determined from Durango apatites in (a) batch 1 and (b) batch 2. The circles represent individual single grain ages with 2σ analytical uncertainties. The shaded areas indicate weighted means and their 2σ standard errors. Grain fragments mounted on copper tape and regular scotch tape are denoted by COT and DST, respectively. The SEM analytical conditions for the Subgroups 1–8 are available in Table 1.

n = 5) as illustrated in Fig. 1. The weighted means of the four subgroups are internally consistent, and also identical to the reference ages listed above. These results suggest that the specified SEM analytical conditions commonly employed for sample description, even for extended chemical mapping at relatively high accelerating energy, cause essentially no effects on the (U–Th)/He systems of the Durango apatite fragments. Fourteen SEM-untreated standard Durango apatite fragments of 90–250 μm (batch 1 and 2) yield a weighted mean age of 31.2 ± 0.6 Ma (MSWD = 0.83), which is also consistent with reference ages for Durango apatite, suggesting that there is no statistical difference between the SEM-treated and SEM-untreated samples.

3.2. Electron–matter interaction simulation

The estimated maximum penetration depth of electrons (=maximum electron depth) increases with the accelerating energy, and is generally consistent with the results of Everhart and Hoff (1971) for lower energy (<15 keV), and approach the model of Wittry and Kyser (1967) for higher energy (>15 keV) (Fig. 2). For a specific accelerating energy of 16.5 keV, which is the condition for our experiments, the maximum electron depth is calculated as ~2 μm. The estimated temperature increase (ΔT) is distinctive in a thin film near the grain surface (depth < ~0.1 μm) with the peak ΔT in the range of ~15 to 250 K, generally increasing with scanning duration and probe current. The ΔT subdues with depth from surface (=d), reaching <25% of the peak ΔT at d = ~0.3 μm (Fig. 3).

For each of the simulated ΔT profiles, we calculated the diffusive redistribution of [He] and resulting f_{He} (fractional He loss) using a finite difference method. For these calculations, the following conditions were assumed: (1) [He] is homogeneous before heating; (2) ΔT is constant in the d interval of 0–0.1 μm, and linearly decreases in 0.1–0.3 μm reaching zero at d = 0.3 μm; and (3) He diffusion follows the

Table 2
(U–Th)/He data for the Durango apatite from the first batch.

	Sample	U	Th	Sm	^{4}He	(U-Th)/He Age	2σ
	Name	[ng]	[ng]	[ng]	[fmol]	[Ma]	[Ma]
Subgroup 1	ApD0102	0.003	0.062	0.050	3.24	33.4	4.4
	ApD0105	0.019	0.385	0.313	18.8	31.6	2.0
	ApD0106	0.054	1.10	0.893	52.8	30.9	1.8
	ApD0107	0.067	1.16	0.875	55.4	30.0	1.8
	ApD0108	0.092	1.80	1.38	86.5	30.8	1.8
	Weighted Mean					30.9	0.9
	MSWD					0.68	
Subgroup 2	ApC0204	0.056	1.13	0.944	54.9	31.3	1.9
	ApC0205	0.005	0.094	0.060	4.64	31.1	2.2
	ApC0206	0.016	0.333	0.270	16.3	31.7	2.1
	ApC0208	0.191	3.29	2.49	160	30.5	1.9
	ApC0209	0.119	2.40	1.98	116	31.0	2.0
	ApC0210	0.052	0.989	0.779	50.7	32.6	2.0
	Weighted Mean					31.3	0.8
	MSWD					0.53	
Subgroup 3	ApD0304	0.010	0.218	0.175	10.8	32.1	2.2
	ApD0305	0.034	0.628	0.500	30.2	30.5	2.0
	ApD0307	0.175	3.63	2.98	172	30.8	2.0
	ApD0309	0.166	3.04	2.21	147	30.6	2.0
	ApD0310	0.082	1.44	1.07	70.2	30.7	2.0
	Weighted Mean					30.9	0.9
	MSWD					0.40	
Subgroup 4	ApC0404	0.032	0.629	0.495	30.03	30.6	2.1
	ApC0405	0.009	0.201	0.157	10.0	32.9	3.1
	ApC0406	0.037	0.761	0.599	35.8	30.4	2.1
	ApC0407	0.143	2.99	2.34	142	30.8	1.9
	ApC0408	0.112	2.27	1.85	106	30.0	2.0
	ApC0409	0.079	1.63	1.35	75.4	30.0	3.6
	ApC0410	0.098	1.98	1.52	99.4	32.4	1.9
	Weighted Mean					30.7	0.9
	MSWD					0.59	
SEM-untreated Durango Apatite	DUR-Ap-U01	0.167	3.51	2.72	168	31.1	1.9
	DUR-Ap-U02	0.182	3.62	3.00	175	31.0	1.9
	DUR-Ap-U03	0.118	2.03	1.52	101	31.0	2.0
	DUR-Ap-U04	0.096	2.01	1.60	98.6	31.9	1.9
	DUR-Ap-U05	0.057	1.17	0.935	60.4	33.4	2.3
	DUR-Ap-U06	0.091	1.61	1.22	79.3	31.1	2.0
	DUR-Ap-U07	0.151	3.08	2.49	151	31.6	3.8
	DUR-Ap-U08	0.076	1.35	1.04	62.6	29.2	3.9
	DUR-Ap-U09	0.065	1.17	0.865	53.7	28.9	3.5
	Weighted Mean					31.3	0.8
	MSWD					0.90	

Table 3
(U–Th)/He data for the Durango apatite from the second batch.

	Sample	U	Th	Sm	^{4}He	(U-Th)/He Age	2σ
	Name	[ng]	[ng]	[ng]	[fmol]	[Ma]	[Ma]
Subgroup 5	A1Ap1	0.197	4.03	3.26	190	30.4	2.7
	A1Ap2	0.203	3.99	3.04	201	32.4	2.7
	A1Ap3	0.130	2.25	1.69	109	30.4	2.2
	A1Ap4	0.108	2.08	1.74	103	31.7	2.3
	A1Ap5	0.184	3.63	3.02	170	30.1	2.7
	A1Ap6	0.128	2.30	2.07	121	33.1	3.1
	A1Ap7	0.158	2.65	2.08	136	32.0	2.6
	A1Ap8	0.133	2.58	2.01	123	30.5	2.7
	Weighted Mean					31.2	0.9
	MSWD					0.66	
Subgroup 6	A2Ap1	0.186	3.20	2.48	152	29.8	2.1
	A2Ap2	0.311	5.66	3.78	275	30.8	2.4
	A2Ap3	0.318	5.99	4.67	303	32.2	2.7
	A2Ap4	0.123	2.43	1.88	109	28.7	2.0
	A2Ap5	0.063	1.23	1.01	58.3	30.4	2.2
	A2Ap6	0.283	5.27	4.26	253	30.5	3.0
	Weighted Mean					30.2	0.9
	MSWD					1.0	
Subgroup 7	A3Ap1	0.109	1.88	1.58	94.6	31.5	2.4
	A3Ap2	0.090	1.85	1.54	88.4	31.0	2.3
	A3Ap3	0.076	1.40	1.17	69.9	31.5	2.4
	A3Ap4	0.047	0.927	0.78	43.1	29.9	2.2
	A3Ap5	0.064	1.31	1.08	61.0	30.0	2.4
	Weighted Mean					30.8	1.0
	MSWD					0.48	
Subgroup 8	A4Ap1	0.119	2.35	2.02	108	29.6	2.6
	A4Ap2	0.253	4.74	3.97	231	31.0	2.3
	A4Ap3	0.121	2.51	2.06	121	31.0	2.2
	A4Ap4	0.139	2.81	2.31	139	31.8	3.2
	A4Ap5	0.052	1.05	0.86	48.3	29.6	2.3
	Weighted Mean					30.5	1.1
	MSWD					0.55	
SEM-untreated Durango apatite	DurAp1	0.124	2.50	2.00	122	31.5	2.9
	DurAp2	0.095	1.59	1.29	76.8	30.1	2.4
	DurAp3	0.101	1.84	1.39	92.9	31.9	2.5
	DurAp4	0.085	1.54	1.10	72.3	29.7	2.1
	DurAp5	0.209	3.77	2.50	190	31.9	2.1
	Weighted Mean (±2σ)					31.0	1.1
	MSWD					0.84	

Arrhenius relationship with diffusion parameters of $E_a = 32.9$ kcal/mol and $D_0 = 50$ cm^2/s (Farley, 2000). The calculated f_{He} is proportional to Ip (probe current) and t (scanning duration) simply because ΔT is enhanced by these parameters (Fig. 4). The resulting f_{He} is less than ~1% for a grain with a thickness larger than 10 μm, even at the most extreme conditions described in this study ($Ip = 1000$ nA, $t = 120$ min). For practical grain dimensions appropriate for conventional (U-Th)/He dating (thickness > ~50 μm), the f_{He} values are estimated to be less than 0.4 % (Fig. 4). To simulate He diffusion from grains that experienced alpha recoil loss, we used an alternative initial [He] profile with a linear increase of [He] within 20 μm from the grain surface, and constant where d > 20 μm. Within the depth where the ΔT is significant (d = 0–0.3 μm), the resulting f_{He} values are at least an order of magnitude smaller than the results from the constant initial [He] profiles. Two different sets of diffusion parameters of Shuster et al. (2003) and Cherniak et al. (2009) yielded f_{He} values indistinguishable from the results obtained from Farley's (2000) diffusion parameters discussed above. Therefore, the calculated f_{He} values from various cases are well within the range of analytical uncertainties for the Durango apatite (U–Th)/He ages, suggesting essentially no detectable helium loss during regular SEM analysis.

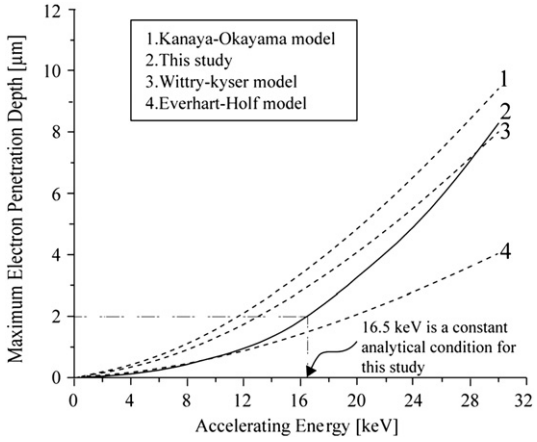

Fig. 2. Comparison of maximum depth as a function of accelerating energy in our model (solid curve 2) with others (dashed curves 1, 3 and 4). The maximum electron depth is proportional to the accelerating energy (=EHT target) for all models. For a specific accelerating energy of 16.5 kV, which is the condition for our experiments, the electron-matter interaction model of this study yields a maximum electron penetration depth of ~2 μm.

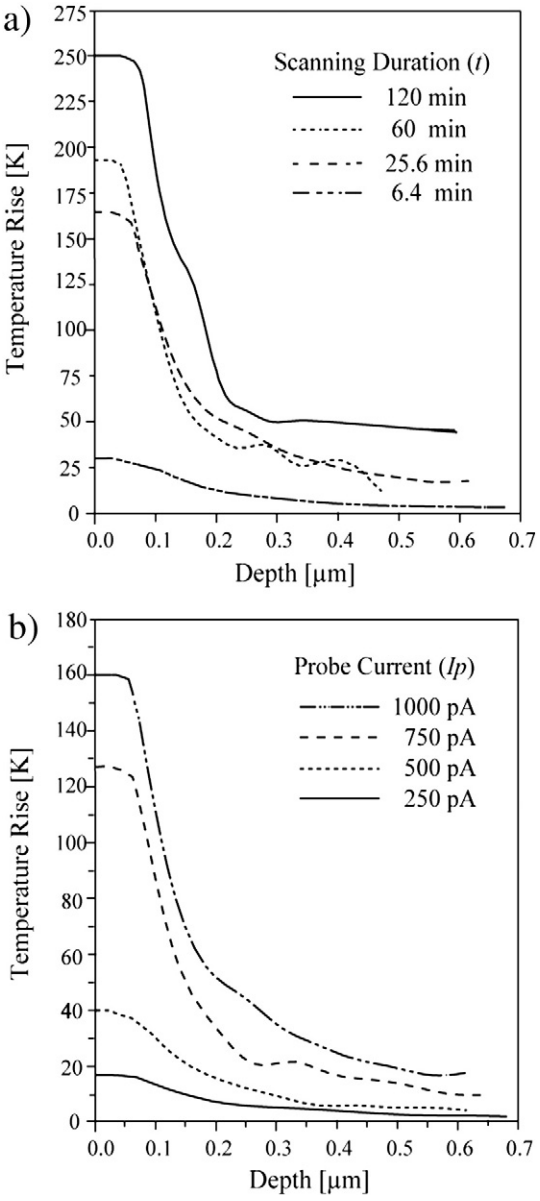

Fig. 3. Calculated temperature rise (ΔT) for (a) different SEM scanning durations at a constant probe current of 1000 pA, and (b) different probe currents at a constant scanning duration of 25.6 min. An accelerating voltage of 16.5 kV was used for both simulations. The calculated ΔT is high near the grain surface, then diminishes rapidly with depth.

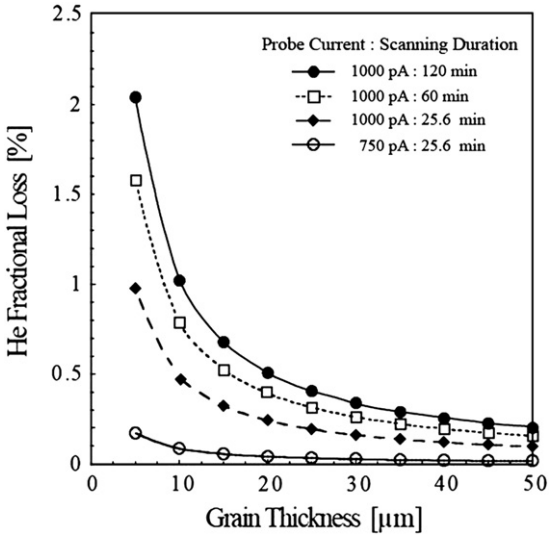

Fig. 4. Fractional loss of He in Durango apatite versus increasing dimensions. The ΔT profiles specified for SEM analytical conditions (Fig. 3) were used for these calculations. The closed circles represent the estimated range of f_{He} in apatite grains for an extended scanning duration (120 min) at a maximum probe current (1000 pA), illustrating that the maximum loss of He is merely 1% even for a very small grain thickness of ~10 μm. The open circles represent the estimated range of f_{He} for a short scanning duration (25.6 min) and a low probe current (750 pA), indicating the fractional loss of He is less than 0.1% for a grain thickness > 10 μm. The calculated He fractional loss for probe currents of 250 pA and 500 pA is essentially identical to zero.

3.3. Implications for thermochronology

Apatite grains with thicknesses smaller than ~50 μm are avoided for (U–Th)/He dating primarily because such grains are subject to significant alpha recoil loss, therefore requiring large corrections which cause significant errors in the calculated (U–Th)/He ages. As described above, the SEM-induced diffusive loss of He for such apatite samples is negligible.

A notable situation is that SEM analysis is frequently applied to K-feldspar before *in situ* $^{40}Ar/^{39}Ar$ dating. Although we have not conducted a systematic evaluation of SEM-induced ΔT in K-feldspar, the ΔT in this mineral is likely to be even lower than in apatite because the thermal conductivity of K-feldspar is in the range of 2.30–2.68 W m^{-1} K^{-1}, which is almost double the value for apatite (1.33 W m^{-1} K^{-1}). Assuming the same T profiles, and using two sets of Ar diffusion parameters for K-feldspar (Foland, 1974; Wartho et al., 1999), we calculated an Ar fractional loss (f_{Ar}) that is less than ~0.01 % for the same grain dimensions (>5 μm) specified for apatite He diffusion modeling. Furthermore, because the typical dimensions of K-feldspar used for the *in situ* approach are larger than ~30–100 μm, which is the typical linear dimension of analytical volume (Hodges et al., 1994; Kelley, 1995; Kramar et al., 2001; Augier et al., 2005; Hudgins et al., 2008; Sherlock et al., 2008), the f_{Ar} in the entire K-feldspar grain would be very small for practical applications. These results suggest that the diffusive Ar loss in K-feldspar during typical SEM analysis is even less significant than for He diffusion in apatite, confirming that the routine SEM usage is not a concern for *in situ* $^{40}Ar/^{39}Ar$ dating of K-feldspar.

Meteoritic samples introduce a potential circumstance where SEM analysis could cause meaningful disturbance because extensive SEM analysis is required to identify phosphates (merrillite and apatite) and to describe the detailed morphological features for successful (U–Th)/He dating (Min et al., 2003, 2004; Min and Reiners, 2007). Because phosphate grains in shocked meteorites (e.g., Martian meteorites) have many intra-grain fractures, their diffusion domains are much smaller than the whole grains, therefore an extended SEM analysis can cause more significant diffusive He loss for such meteoritic phosphate fragments. The diffusion radii of some such phosphate fragments are estimated to be <5 μm (Min et al., 2004; Min and Reiners, 2007; Min et al., 2013) which can potentially cause diffusive He loss of more than ~2 % at extreme SEM analytical conditions (Fig. 4). However, this thermal effect can be avoided by using relatively large (>50 μm) fragments because the SEM-induced ΔT is limited to a very shallow depth from the grain surface.

Another notable situation where SEM analysis could cause meaningful disturbance occurs when examining ion implanted samples using SEM. The procedure of ion implantation followed by isothermal heating experiments is frequently used to describe the diffusion properties of implanted elements or isotopes in target materials (Cherniak et al., 2009). During He implantation into apatite, the depth of He injection is limited to the shallow volume near the mineral surface, with the implantation depth normally in the order of a few micrometers, or even less than one micrometer (Ouchani et al., 1998; Cherniak et al., 2009). Because the SEM analysis can cause

considerable ΔT near the grain surface, the injected He profile in the grain can be significantly modified. Therefore, caution is required if such He-implanted apatite grains are examined under SEM before diffusion experiments. The probable best way to circumvent the potential problems is to undertake SEM analysis after diffusion experiments or make a separate set of samples for a SEM investigation.

4. Summary

In this paper, we investigated the potential causal effect of SEM analysis on He diffusion in apatite using the two independent approaches of (1) direct determination of (U–Th)/He ages of SEM-treated apatite fragments, and (2) electron-matter interaction simulation combined with diffusion modeling. The Durango fragments, divided into eight subgroups for systematic evaluation of multiple parameters of grain size, mounting material, SEM probe current and scanning duration, yielded internally and externally consistent (U–Th)/He ages. The electron-matter interaction simulation yielded ΔT–d profiles with maximum ΔT within the shallow depth from the grain surface (<~0.1 μm), followed by decreasing ΔT with depth. Under the regular SEM analytical conditions, the f_{He} values calculated from the simulated ΔT profiles are less than 0.4% for typical apatite grains with thicknesses of >~50 μm. These results suggest that the SEM electron beam leads to only minor ΔT, causing no detectable diffusive He loss for most of the apatite samples to be used for (U–Th)/He dating.

Acknowledgements

We thank Annette Farah and Arkin Buyukozturk for lab assistance, Wenyuan Zhang for computer simulation of He diffusion, and Ann Heatherington for constructive discussions. Constructive comments from two anonymous reviewers and Klaus Mezger (Editor) greatly improved the original manuscript. JS sincerely appreciates the financial support from Dr. Shengbiao Hu during her stay at University of Florida.

Appendix

Following SEM analysis, all grain fragments were retrieved and individually wrapped in ~500 μm × 500 μm (diameter × length) platinum tubes for (U-Th)/He age determination. Each sample packet was loaded in a ~3 mm-deep well in a stainless steel planchette, and heated using a diode laser at 7 Amp for 3 min. To ensure complete release of ^{4}He in the batch 1 samples, each sample packet was re-heated for a few minutes after the primary heating. Subsequent to the completion of the first batch of samples, the He analytical system at the University of Florida was automated, enabling us to analyze the second batch of samples with a more stable and time-efficient mode. Two re-extractions were performed for the second batch of samples. In both cases, the final re-extraction steps yielded less than 1% of the total ^{4}He. The extracted gas was spiked with a known amount of 99.99% ^{3}He, purified with a NP-10 getter, and then analyzed using a quadrupole mass spectrometer (QMS) with a channeltron multiplier. Following ^{4}He measurements, the degassed sample packets were retrieved, transferred to Teflon vials, mixed with a shot of spike and dissolved with ~5% nitric acid at ~120 °C. The abundances of U, Th and Sm were determined using a Thermo-Finnigan Element2 Inductively Coupled Plasma Mass Spectrometer (ICP-MS).

References

Augier, R., Agard, P., Monie, P., Jolivet, L., Robin, C., Booth-Rea, G., 2005. Exhumation, doming and slab retreat in the Betic Cordillera (SE Spain): *in situ* ^{40}Ar/^{39}Ar ages and P-*T*-*d*-*t* paths for the Nevado–Filabride complex. Journal of Metamorphic Geology 23, 357–381.

Boyce, J.W., Hodges, K.V., 2005. U and Th zoning in Cerro de Mercado (Durango, Mexico) fluorapatite: Insights regarding the impact of recoil redistribution of radiogenic ^{4}He on (U–Th)/He thermochronology. Chemical Geology 219, 261–274.

Cherniak, D.J., Watson, E.B., Thomas, J.B., 2009. Diffusion of helium in zircon and apatite. Chemical Geology 268, 155–166.

Chew, D.M., Sylvester, P.J., Tubrett, M.N., 2011. U–Pb and Th–Pb dating of apatite by LA-ICPMS. Chemical Geology 280, 200–216.

Egerton, R., Li, P., Malac, M., 2004. Radiation damage in the TEM and SEM. Micron 35, 399–409.

Everhart, T., Hoff, P., 1971. Determination of kilovolt electron energy dissipation vs penetration distance in solid materials. Journal of Applied Physics 42, 5837–5846.

Farley, K.A., 2000. Helium diffusion from apatite: general behavior as illustrated by Durango fluorapatite. Journal of Geophysical Research 105, 2903–2914.

Flude, S., Sherlock, S., Lee, M., Kelley, S.P., 2010. The effect of SEM imaging on the Ar/Ar system in feldspars. Abstract V51C-2215 presented at 2010 Fall Meeting, AGU, San Francisco, Calif., 13–17 Dec.

Foland, K.A., 1974. Ar^{40} diffusion in homogenous orthoclase and an interpretation of Ar diffusion in K-feldspars. Geochimica et Cosmochimica Acta 38, 151–166.

Hodges, K.V., Harries, W.E., Bowring, S.A., 1994. ^{40}Ar/^{39}Ar age gradients in micas from a high-temperature-low-pressure metamorphic terrain: Evidence for very slow cooling and implications for the interpretation of age spectra. Geology 22, 55–58.

Hudgins, J.A., Spray, J.G., Kelley, S.P., Korotev, R.L., Sherlock, S.C., 2008. A laser probe ^{40}Ar/^{39}Ar and INAA investigation of four Apollo granulitic breccias. Geochimica et Cosmochimica Acta 72, 5781–5798.

Kelley, S., 1995. Ar–Ar dating by laser microprobe. Microprobe Techniques in the Earth Sciences 6, 327–358.

Kramar, N., Cosca, M.A., Hunziker, J.C., 2001. Heterogeneous ^{40}Ar* distributions in naturally deformed muscovite: in situ UV-laser ablation evidence for microstructurally controlled intragrain diffusion. Earth and Planetary Science Letters 192, 377–388.

McDowell, F.W., McIntosh, W.C., Farley, K.A., 2005. A precise 40Ar–39Ar reference age for the Durango apatite (U–Th)/He and fission-track dating standard. Chemical Geology 214, 249–263.

Min, K., Reiners, P.W., 2007. High-temperature Mars-to-Earth transfer of meteorite ALH84001. Earth and Planetary Science Letters 260, 72–85.

Min, K., Farley, K.A., Renne, P.R., Marti, K., 2003. Single grain (U–Th)/He ages from phosphates in Acapulco meteorite and implications for thermal history. Earth and Planetary Science Letters 209, 323–337.

Min, K., Reiners, P.W., Nicolescu, S., Greenwood, J.P., 2004. Age and temperature of shock metamorphism of Martian meteorite Los Angeles from (U-Th)/He thermochronometry. Geology 32, 677–680.

Min, K., Reiners, P.W., Wolff, J., Mundil, R., Winters, L.R., 2006. (U–Th)/He dating of volcanic phenocrysts with high-U–Th inclusions, Jemez Volcanic Field, New Mexico. Chemical Geology 227, 223–235.

Min, K., Reiners, P.W., Shuster, D.L., 2013. (U–Th)/He ages of phosphates from St. Severin LL6 chondrite. Geochimica et Cosmochimica Acta 100, 282–296.

Mirkarimi, P.B., Stearns, D.G., Baker, S.L., Elmer, J.W., Sweeney, D.W., Gullikson, E.M., 2002. Method for repairing Mo/Si multilayer thin film phase defects in reticles for extreme ultraviolet lithography. Journal of Applied Physics 91, 81–89.

Nouiri, A., Chaguetmi, S., Belabed, N., 2006. Monte Carlo model of the temperature rise at a GaAs surface under an electron beam. Surface and Interface Analysis 38, 1153–1157.

Ouchani, S., Dran, J.C., Chaumont, J., 1998. Exfoliation and diffusion following helium ion implantation in fluorapatite: implications for radiochronology and radioactive waste disposal. Applied Geochemistry 13, 707–714.

Randolph, S., Fowlkes, J., Rack, P., 2005. Effects of heat generation during electron-beam-induced deposition of nanostructures. Journal of Applied Physics 97, 124312.

Sherlock, S.C., Jones, K.A., Park, R.G., 2008. Grenville-age pseudotachylite in the Lewisian: laserprobe ^{40}Ar/^{39}Ar ages from the Gairloch region of Scotland (UK). Journal of the Geological Society 165, 73–83.

Shuster, D.L., Farley, K.A., Sisterson, J.M., Burnett, D.S., 2003. Quantifying the diffusion kinetics and spatial distributions of radiogenic ^{4}He in minerals containing proton-induced ^{3}He. Earth and Planetary Science Letters 217, 19–32.

Spiegel, C., Kohn, B., Belton, D., Berner, Z., Gleadow, A., 2009. Apatite (U–Th–Sm)/He thermochronology of rapidly cooled samples: the effect of He implantation. Earth and Planetary Science Letters 285, 105–114.

Talmon, Y., Thomas, E.L., 1977. Beam heating of a moderately thick cold stage specimen in the SEM/STEM. Journal of Microscopy 111, 151–164.

Talmon, Y., Thomas, E.L., 1978. Electron beam heating temperature profiles in moderately thick cold stage STEM/SEM specimens. Journal of Microscopy 113, 69–75.

Wartho, J.-A., et al., 1999. Direct measurement of Ar diffusion profiles in a gem-quality Madagascar K-feldspar using the ultra-violet laser ablation microprobe (UVLAMP). Earth and Planetary Science Letters 170, 141–153.

Wittry, D.B., Kyser, D.F., 1967. Measurement of diffusion lengths in direct-gap semiconductors by electron-beam excitation. Journal of Applied Physics 38, 375–382.

Wolf, R., Farley, K., Silver, L., 1996. Helium diffusion and low-temperature thermochronometry of apatite. Geochimica et Cosmochimica Acta 60, 4231–4240.

Wolf, R., Farley, K., Silver, L., 1997. Assessment of (U–Th)/He thermochronometry: the low-temperature history of the San Jacinto mountains, California. Geology 25, 65–68.

Zeitler, P.K., Herczeg, A.L., McDougall, I., Honda, M., 1987. U–Th–He dating of apatite: a potential thermochronometer. Geochimica et Cosmochimica Acta 51, 2865–2868.